Geochemistry Geophysics Geosystems G3
AN ELECTRONIC JOURNAL OF THE EARTH SCIENCES
Published by AGU and the Geochemical Society

Article
Volume 6, Number 9
27 September 2005
Q09015, doi:10.1029/2005GC000928
ISSN: 1525-2027

River networks of southern Africa: Scaling laws governing their geometry and deviations from scaling

Jacek Stankiewicz and Maarten J. de Wit

CIGCES, Department of Geological Science, University of Cape Town, Private Bag, Rondebosch 7700, South Africa (maarten@cigces.uct.ac.za)

[1] Africa is tectonically and hypsometrically different to all other continents and therefore provides a unique natural laboratory for the study of river network geometry. Southern Africa is one of the more unusual geomorphological regions of this continent, hence our interest in the geometry of the rivers draining this region. The 14 river basins analyzed here come from the larger networks of the Orange and Limpopo rivers, as well as from the southernmost section of the continent where rivers meander through an exhumed belt of folded Paleozoic mountains. Basic scaling laws, such as Horton's laws and Hack's law, hold for the rivers studied here, but the parameters governing these relationships vary between networks. A strong inverse correlation between Horton's ratio of stream numbers and mean source stream slope is observed. We believe this is the first time such a relation has been reported. Horton's ratio of basin areas is proportional to that of stream numbers but always greater than it; this contradicts existing models that equate the two parameters. An expression for the ratio of stream lengths in terms of the ratio of stream numbers is derived theoretically and verified for the available data. The parameter governing Hack's law, h, varies not only between networks but also with scale inside each network. Existing models provide up to four scaling regimes. Given the spatial resolution of this study, the two regimes at the middle scales are visible here. These are termed the short-range and randomness regimes, with a crossover occurring at a drainage area of approximately 800 km^2. The values for h in the smaller short-range regime have an inverse correlation with the roughness of the topography. Observed values for h imply basins appear more elongated with increasing area; this would be more pronounced in rivers draining a smooth topography. In the randomness regime the values of h are lower, mostly between 0.5 and 0.6, with a weak positive correlation to topography roughness. This range of h corresponds to self-similar basins, but a more detailed analysis of individual stream fractality is necessary before such a conclusion can be made.

Components: 9711 words, 17 figures, 3 tables.

Keywords: Africa; continent; fractal analysis; geomorphology; river networks.

Index Terms: 1824 Hydrology: Geomorphology: general (1625); 1848 Hydrology: Monitoring networks; 8175 Tectonophysics: Tectonics and landscape evolution.

Received 26 January 2005; **Revised** 5 June 2005; **Accepted** 4 August 2005; **Published** 27 September 2005.

Stankiewicz, J., and M. J. de Wit (2005), River networks of southern Africa: Scaling laws governing their geometry and deviations from scaling, *Geochem. Geophys. Geosyst.*, *6*, Q09015, doi:10.1029/2005GC000928.

1. Introduction to African Topography

[2] Africa (Figure 1) has a unique topography. While elevated regions of other continents can be usually related to tectonic uplift linked to horizontal convergent plate tectonic forces, Africa is host to some of the world's greatest elevated regions despite being mostly (>90%) surrounded by divergent plate margins, and its upper crust being predominantly in a state of extensional stress [*Zoback et al.*, 1989; *Coblentz and Sandiford*, 1994]. The only high elevation region in Africa related to convergent plate boundary stresses is the Atlas mountains in northwest Africa [*Frizon de*

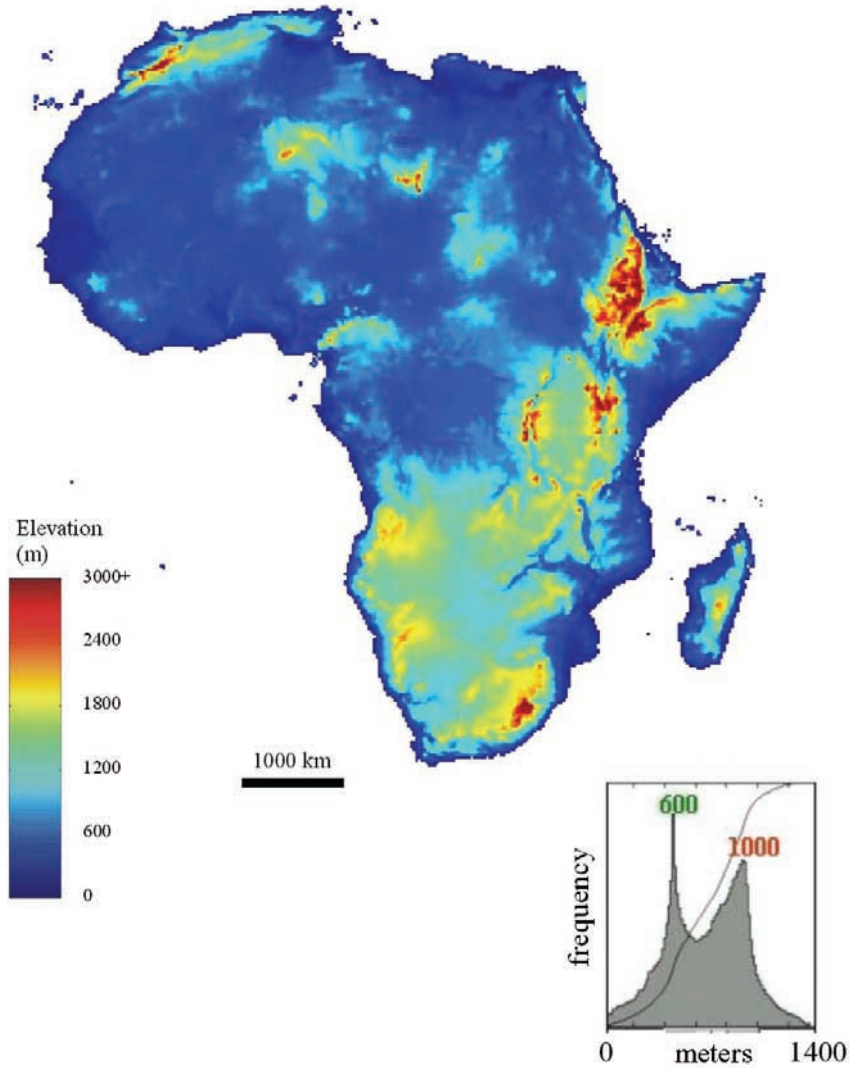

Figure 1. Topography of the African continent. Note the bimodality: the southern and eastern sections are much higher than the central and western parts. A number of basins can also be seen, the Congo and Chad being the most prominent ones. This figure, as well as Figure 5, was constructed using data from the USGS Web site: http://edcdaac.usgs.gov/gtopo30/gtopo30.html. Inset: Elevation frequency histogram based on Figure 3a of *Doucouré and de Wit* [2003].

Lamotte et al., 2000]. Africa's anomalous continental-scale geomorphology was first pointed out by *Holmes* [1944], who termed it the "basin and swell structure." Furthermore, Africa's topography is distinctly bimodal, with central and west Africa being more smooth and low-lying (mostly <500 m) than the southern and eastern sections of the continent which are generally higher that 1000 m [e.g., *Brown and Gilder*, 1980]. *Doucouré and de Wit* [2003] computed a histogram of Africa's elevation (their Figure 3a, modified here as inset in Figure 1), on which 2 peaks corresponding to heights of ~600 and 1000 m are clear to see. This demonstrates the bimodality statistically. The age and the origin of this topography is a subject of some controversy. Some believe all these features to be Cenozoic in age [e.g., *Buckle*, 1978; *Burke*, 1996; *Partridge and Maud*, 1987], relating to mantle upwellings [e.g., *Burke*, 1996; *Lithgow-Bertelloni and Silver*, 1998]. Others acknowledge the influence of paleo-horizontal plate tectonic forces in formations of these features [e.g., *Fairhead*, 1988; *Sahagian*, 1988]. A gravity anomaly study by *Doucouré and de Wit* [2003] suggests that both strong topographic bimodality and basin and swell structures were already present in the Cretaceous.

[3] In the absence of significant Mesozoic-Cenozoic orogenic uplift, Africa's epeirogenic topography might be expected to produce river

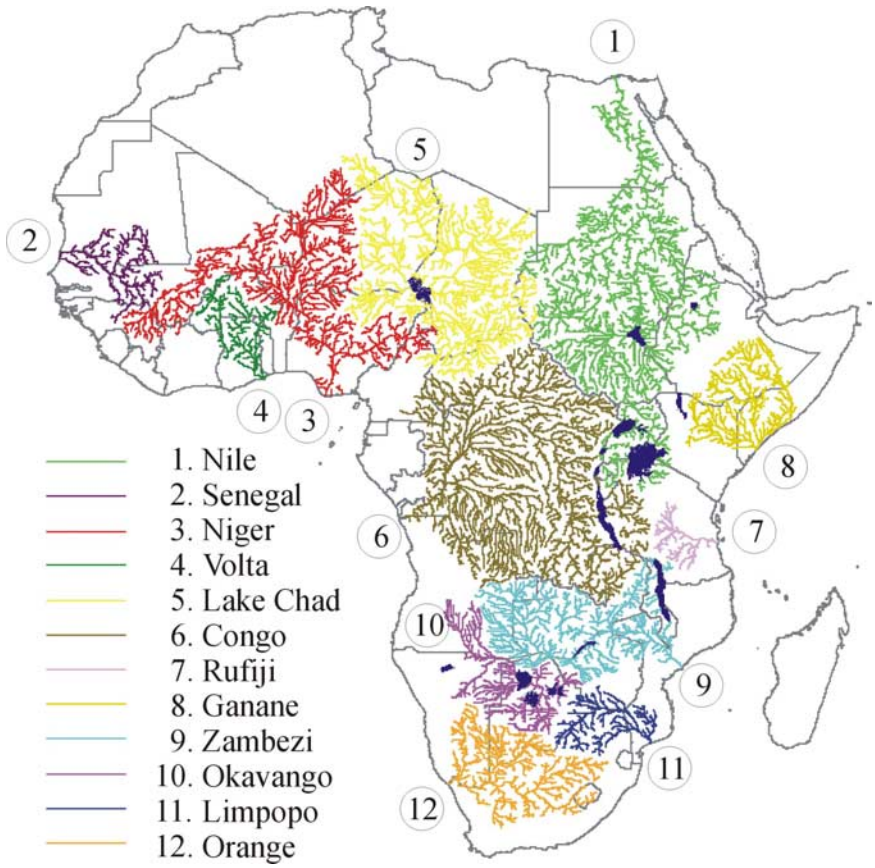

Figure 2. Largest drainage basins in Africa. Note that two of them (Chad and Okavango) are landlocked. This figure was constructed using the CIGCES African river database based on digitized maps from De Beers Group, Centurion.

networks different to ones on all other continents, and it does (Figure 2). A number of rivers flow away from the coast they are closest to, and what would appear to have been the logical outlet (e.g., Niger, Zambezi, Orange). These have been suggested to be plume-related drainages formed above mantle hot spots (e.g., hot upwelling mantle [*Cox*, 1989]). There are a number of plume-related failed rifts in Africa, and these often become major river valleys (e.g., the Benue tributary of the Niger in Central Africa and the Limpopo river in southern Africa). Africa thus presents a fascinating natural laboratory of river networks apparently different to anywhere else in the world. A number of basins are landlocked (Okavango and Chad being the largest ones, and the Congo basin until recently (J. Stankiewicz and M. J. de Wit, The east-flowing Congo River and implications for the evolution of African River Basins, submitted to *Journal of African Earth Sciences*, 2005)), though this is not unique to Africa (e.g., Caspian Sea).

[4] In this study we concentrate on the southern section of the African continent, perhaps the more unusual part of the bimodal topography [*Doucouré and de Wit*, 2003]. We investigate how the unique landscape and bedrock structure of the region affects the self-organization of river networks draining the subcontinent.

2. Drainage Systems of Southern Africa

[5] One way to illustrate the distribution of topography elevation is by plotting hypsometric functions. These express what percentage of the surface area is above a given elevation. It is convenient to deviate from convention and plot the independent variable (elevation) of the vertical axis; that way the curve can be thought of as an average maximal river profile that would drain the topography. Figure 3 shows the hypsometric curves for the entire Africa (black), southern Africa (blue), and an approximate curve usually found on other continents (red, from Figure 25 of *Burke* [1996]). It has been often mentioned in literature that the curve for Africa is mostly above the curve for other continents [e.g., *Cogley*, 1987; *Burke*, 1996].

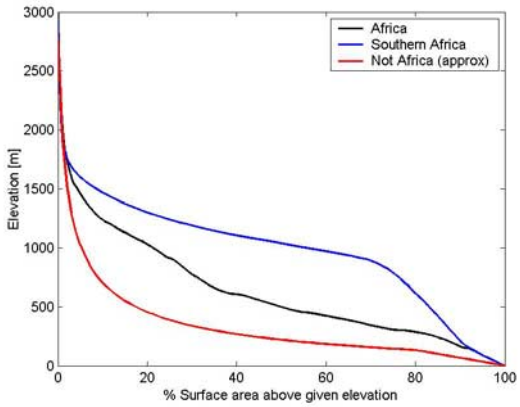

Figure 3. Hypsometric curves for Africa (black) and southern Africa (blue) and approximate curve for other continents (red [from *Burke*, 1996]).

From the figure presented here, it appears that this anomaly is mostly due to the high topography in southern Africa, hence our interest in that section of the continent.

[6] One of the main features of the region's geomorphology can be seen by looking at the drainage map of southern Africa (Figure 4): the Great Escarpment, stretching from the Atlantic coast near Namibia, to the Limpopo basin near the boundaries of South Africa with Zimbabwe and Moçambique, in an arc approximately 200 km from the coast. All the drainage inland of this divide eventually joins either the Orange or the Limpopo rivers and enters the Atlantic at Oranjemund or the Indian Ocean near Xai-Xai, respectively (Figure 4).

[7] The Orange is the major river in the region; it is the fifth largest river in Africa, both in terms of mainstream length (2150 km) and drainage area (1,040,000 km^2). Its major tributaries drain different geological and climatic terrains. Large part of the drainage comes from the Orange-Vaal system sources in high ground inland of the Drakensberg escarpment. This high ground (reaching 3482 m at its highest point, Thabana Ntlenyana in Lesotho) has been suggested to be inherited from a deep mantle plume at ~180 Ma just prior to the breakup of Gondwana [*White and McKenzie*, 1989]. The fact that the Orange has its sources just 150 km west of the Indian Ocean, but flows to the Atlantic 1400 km away, has been seen as a case of drainage away from the new (Indian) ocean, supporting this paleo-plume hypothesis [*Cox*, 1989]. The second largest river in the area, the Limpopo, flows through a similar geological terrain, but in the opposite direction, reaching the Indian Ocean through a delta in Moçambique. *Cox* [1989] suggests that the Limpopo drainage is rift-inherited, related to the failed spreading axis in the Kalahari postulated by *Reeves* [1972, 1978]. *Du Toit* [1933] suggested that the Limpopo was originally linked with the Okavango, a theory supported by *Wellington* [1955] who attributed the drainage evolution to stream capture.

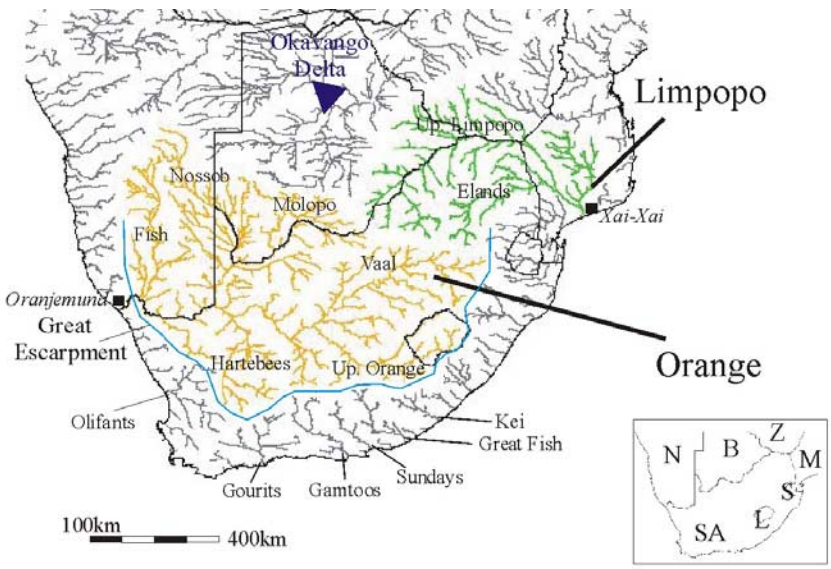

Figure 4. Drainage pattern of southern Africa, from the CIGCES African river database. Pale blue line marks the Great Escarpment. Inset shows the countries in the region: N, Namibia; B, Botswana; Z, Zimbabwe; M, Moçambique; S, Swaziland; L, Lesotho; SA, South Africa.

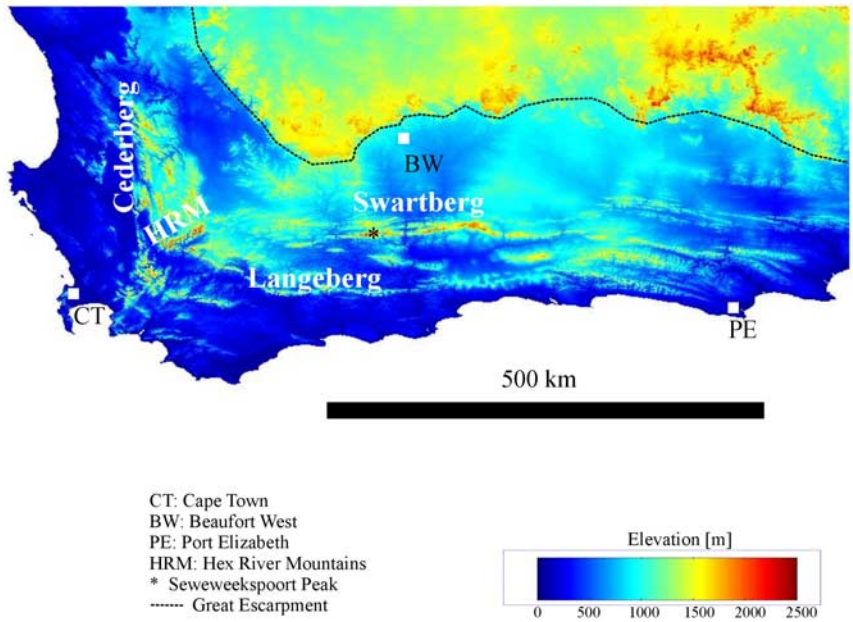

Figure 5. Topography of the Cape Fold Belt and its surroundings.

[8] The Fish River flows south through the arid Namibia, and the only perennial part of the network is the few kilometers upstream from its confluence with the Orange. The most dramatic feature of this network is the famous Fish River Canyon in the river's lower reaches. There the river has cut into the horizontal quartzitic sandstones and shales of the Eocambrian Nama Group (500–700 Ma) to reach the underlying Precambrian schist and granite gneiss of the Namaqua complex (1000–1200 Ma [*Buckle*, 1978]). In places the canyon is over 500 m deep.

[9] The Molopo and Nossob rivers drain (technically speaking) the Kalahari basin. Neither network has a record of permanent flow during living human history [*Bootsman*, 1997]. When water is transported in the channels, overland flow never reaches the Orange river; transport takes place by groundwater. The two networks are therefore not strictly tributaries of the Orange, but have been included in the analysis nonetheless. The presence of river terraces indicates that both these rivers were perennial in past history during more fluvial stages of the recent southern African climate [*de Wit*, 1993].

[10] The Hartebees River, also known as Sak River, is the last major tributary included here. Its headwaters drain north from the southwestern edge of the Great Escarpment across Permian Upper Ecca and Lower Beaufort Group sandstones and shales intruded by thick Jurassic mafic sills. Most of this network is also nonperennial, but as with the Molopo and Nossob, the presence of terraces suggests this has not always been the case. On these terraces there are today a number of "vleis" (local name for wetlands) that characterize the river. Fossil evidence further indicates that as recently as the Middle Miocene (10–15 Ma) the Hartebees flowed through a wet and wooded environment [*de Wit*, 1990, 1993].

[11] The zone between the escarpment and the ocean is drained by rivers approximately perpendicular to the divide. Of the rivers in that band six are of particular interest in this study. They are the Olifants, Gourits, Gamtoos, Sundays, Great Fish and Kei. To reach the coast on their way down from the Great Escarpment they cross a band of mountains ranges known as the Cape Fold Belt (Figure 5). This is the only place in the subcontinent where relatively young fossil mountain ranges (~250 Ma) related to horizontal compressional tectonics are found. The mountains in the belt reach over 2000 m in places, with Seweweekspoort Peak in the Swartberg being the highest point at 2324 m. Other ranges in the belt are the Cederberg, Hex River Mountains, Langeberg and many other smaller ranges. The precursors of these ranges formed during extensive thrusting and folding at ~250 Ma, before they were covered by a substantial thickness of sediment in the Jurassic, and then exhumed again since then [*Tinker and de Wit*, 2004]. Major rivers predating this exhumation

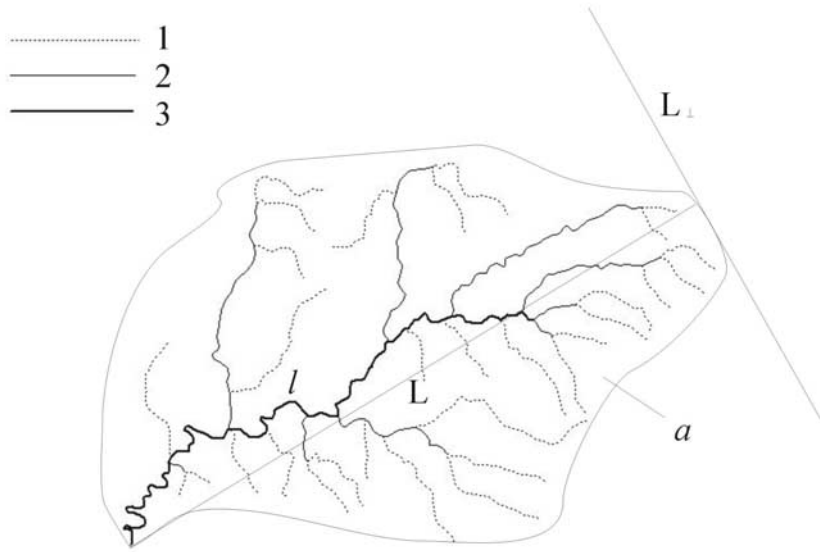

Figure 6. Horton-Strahler ordering scheme and basic basin parameters illustrated on a schematic network.

meander through these mountains. The new river segments have formed in the weaker shale-dominated valleys, leaving the hard Table Mountain Sandstones (often quartzites) as vertical ridges. Lower-order streams then flow down these steep ridges to join the main (higher-order) stream, resulting in a trellis pattern. This environment is not found anywhere else in southern Africa, hence our interest in how and why river network geometry differs between this and other areas.

3. Fractal River Networks

[12] The scale invariance of geological phenomena is one of the first things taught to earth science students. In geological photographs a scale defining object, like a coin or a person, needs to be placed to give an idea of the object's size. For example, given a photograph of a fold without such an object it might be impossible to determine whether it covers 10 cm or 10 km. Objects that have similar properties over a large spectrum of sizes are said to be self-similar over that range. One example of such objects, a coastline, was used by *Mandelbrot* [1967] as he created the concept of fractals.

[13] *Mandelbrot* [1983] went on to show that these fractals abound in nature. *Turcotte* [1992] showed how geology and geophysics are full of such self-similar phenomena. *Dodds and Rothman* [1999] start their study with a claim that if scaling laws abound in nature, river networks stand as an epitome of the phenomenon, as also highlighted by *Rodriguez-Iturbe and Rinaldo* [1997]. Here we first show how rivers can be thought of as fractals, and present the commonly used scaling laws governing their geometry.

3.1. Stream Ordering and Horton's Ratios

[14] A basic tool used in an analysis of river networks is stream ordering. The most widely used scheme was developed by *Strahler* [1957], who based it on a scheme of *Horton* [1945]. In this scheme all stream segments are attached a positive integer number, ω, with higher order implying a larger stream. All source streams (from the source to the first confluence) are given order $\omega = 1$. When two or more streams join, the stream segment downstream from the confluence is assigned the highest of the orders of the contributing streams. If there is more than one highest-order stream, the downstream segment is given order one higher than that highest order. This scheme is illustrated in Figure 6. This figure also shows the basic measurable parameters of a drainage basin. These include the drainage area a marked out by the watersheds of the basin, the mainstream length l in the basin, the length of the basin, L, and its width, $L_\perp$. The stream reaching the outlet of the network obviously has the highest order; this is labeled Ω and is also used to describe the order of the network. Some anomalies can arise if the stream length is not defined explicitly. Horton's original study measured the length of an ω order stream from its formation (confluence of two $\omega - 1$ streams) to the origin of the $\omega + 1$ stream or the outlet, should $\omega = \Omega$. These are referred to as stream segments. Alternatively,

mainstream lengths (from the origin of the lowest-order stream to the end of the ω segment) can be used. Here we used the latter method, as the mainstream lengths gave better correlations than stream segments (see section 4.1).

[15] After a particular network has been ordered using the above scheme, it is possible to calculate the number of streams of a particular order, n, as well as the average stream length and basin area of a given order stream. *Horton* [1945] defined three ratios relating to how these quantities change with order:

$$R_n(\omega) = \frac{n(\omega)}{n(\omega+1)}, \tag{1a}$$

$$R_l(\omega) = \frac{l(\omega+1)}{l(\omega)}, \tag{1b}$$

$$R_a(\omega) = \frac{a(\omega+1)}{a(\omega)}. \tag{1c}$$

Note that the ratios are defined so that they are all greater than unity. Horton also found that all the ratios are independent of the order ω; this would be a requirement for a network to be self-similar. Thus, for example,

$$a(\omega) = (R_a)^{\omega-1} * a(\omega=1), \tag{2a}$$

and therefore

$$\log[a(\omega)] = \log[a(\omega=1)] + (\omega-1)\log(R_a). \tag{2b}$$

Thus plotting mean basin area of a given order on a logarithmic axis as a function of the order will yield a straight line with slope log (R_a). This technique will be used to determine Horton's ratios later on in this study.

[16] Typical values for R_l are between 1.5 and 3.0, and for R_a and R_n between 3.0 and 5.0, though R_a values up to 6.0 have been reported [e.g., *Abrahams*, 1984; *Dodds and Rothman*, 1999]. Values for R_a and R_n are often similar; in fact, *Peckham* [1995] suggested that for self-similar networks an identity $R_a \equiv R_n$ holds. This identity was mathematically derived by *Dodds and Rothman* [1999] using the assumptions of uniform drainage density, and network and stream self-similarity.

3.2. Tokunaga's Ratios

[17] While Horton's ratios can be used to check for self-similarity, and conclusions about real networks can be drawn from the values of Horton's ratios and deviations from them, these ratios do not paint a full picture. All information about low-order streams feeding higher-order streams is lost. To rectify this, *Tokunaga* [1966, 1978, 1984] developed a more detailed way of studying network geometry. Using the Horton-Strahler scheme, $T(\omega_1, \omega_2)$, where $\omega_1 > \omega_2$, is defined to represent the average number of side tributaries of order ω_2 feeding a stream of order ω_1. For self-similar networks first we have

$$T(\omega_1, \omega_2) = T(\omega_1 - \omega_2) = T(\nu). \tag{3}$$

In other words, T is independent of order and is not a function of two variables (ω_1 and ω_2), but of just one variable: the difference between the two orders. Tokunaga's law goes further and states that

$$T(\nu) = T_1 (R_T)^{\nu-1}. \tag{4a}$$

The two network-dependant parameters, T_1 and R_T, can be obtained by plotting logarithms of the ratios $T(\nu)$ as a function of $\nu - 1$, as

$$\log T(\nu) = \log T_1 + (\nu-1)\log R_T. \tag{4b}$$

The slope of this graph corresponds to the log (R_T), and the intercept to log (T_1). *Dodds and Rothman* [1999] show it is possible to express T_1 and R_T in terms of Horton's ratios:

$$R_T = R_l, \tag{5}$$

$$T_1 = R_a - R_l - 2 + 2R_l/R_a. \tag{6}$$

3.3. Hack's Law

[18] An important network geometry scaling law concerns the relationship between stream length, l, and drainage area, a. This was first investigated by *Hack* [1957], who found that

$$l = ca^h, \tag{7}$$

where c is constant of proportionality, and h the scaling exponent, which he found to be approximately 0.6. From a naive geometrical perspective, one would expect this constant to be 1/2. Nearly 50 years after Hack's original study, there is still considerable debate about whether the exponent is, or should be, 1/2. *Ijjasz-Vasquez et al.* [1993] show that deviations from h = 1/2 represent a deviation from self-similarity. *Rigon et al.* [1998] show that networks with h = 1/2 are "far from realistic", and quote a value of h between 0.56 and 0.58 for what they term "feasible" networks. *Dodds and Rothman* [2000] follow up a suggestion by *Mueller*

[1973] that inside a network h changes with scale, and they present a "scaling regime model", with up to 4 scaling regimes. In each of these regimes controls on basin formation are different, and a different value of h should be expected.

[19] The interpretation of the parameters in equation (7) might be of interest. Traditionally, each basin and its subbasins in a network were treated as a data point, and plotted on a logarithmic graph of l as a function of a. This was the method used by *Hack* [1957]. An interesting variation is presented by *Pelletier* [1999], who computes the average stream length and drainage area of all basins of a given order in a network. This results in a number of data points equal to the order Ω of the network.

3.4. Other Scaling Laws and Parameters

[20] One scaling relation that should be mentioned is between the basin's length and its mainstream length:

$$l \sim L^d. \tag{8}$$

This might appear to be a fairly insignificant relation, especially as d is almost always 1.1 [*Maritan et al.*, 1996]. However, *Dodds and Rothman* [2000] show that many river networks can be characterized by universality classes defined by just two parameters: h and d.

[21] There are other parameters which can be calculated for each basin. These include the mean slope of the mainstream (s), and the relief of the basin (r) defined as the difference in elevation between the highest and lowest point. *Tarboton et al.* [1989] investigated the relationship between basin slope and drainage area for 2 basins in North America. The basin areas they used were between 0.2 and 3,000 km^2. These authors found too much scatter when each basin was considered as a data point, and therefore they averaged data from basins with similar areas. Each such bin contained at least 20 individual basins. From this averaged data, they concluded that there exists a power law relationship between the two, albeit with a lot of deviations:

$$s \sim a^x, \tag{9}$$

where x has a value of very close to $-1/2$. *Pelletier* [1999], once again averaging all basins of a specific order, also finds the power law (9) to hold, but for most of the networks in his study the value of x is between -0.34 and -0.41. The basins in his study vary in size from 0.01 to 10,000 km^2, i.e., a much greater range than *Tarboton et al.* [1989]. Interestingly, the results of those studies, as well as of more recent ones [*Rodriguez-Iturbe and Rinaldo*, 1997; *Schorghofer and Rothman*, 2001, 2002], show that the slope-area relation does not hold at the lowest scales considered in each of these studies. As these "lowest scales" differ significantly in these analyses, one is led to believe this is not a real threshold, but depends on the resolution used.

Table 1. Basic Geometric Properties of the 14 Rivers Used in This Study[a]

River	Basin Area, km^2	Main Stream Length, km	Ω	n(ω = 2)
Fish	109,000	854	6	367
Nossob	173,000	941	6	588
Molopo	151,000	846	7	485
Vaal	157,000	935	6	503
Upper Orange	102,000	813	6	201
Hartebees	104,000	624	7	318
Olifants	74,000	572	6	157
Gourits	54,000	330	6	110
Gamtoos	41,000	502	5	88
Sundays	27,000	347	5	41
Great Fish	36,000	503	5	70
Kei	23,000	291	5	34
Upper Limpopo	286,000	1292	6	621
Elands	95,000	678	6	202

[22] *Pelletier* [1999] also investigates the relationship between basin relief and basin area. Once again, a power law dependence is observed:

$$r \sim a^y \tag{10}$$

with the observed value of y between 0.17 and 0.38.

4. Analysis of River Basins in Southern Africa

[23] Rivers discussed in section 2 were used in this analysis. In order to have basin sizes of similar order of magnitude, the 6 subnetworks of the Orange (Fish, Nossob, Molopo, Vaal, Upper Orange and Hartebees) were treated separately. Similarly, the Limpopo was subdivided into Upper Limpopo and Elands (Figure 4). The 6 Cape Fold Belt rivers (Olifants, Gourits, Gamtoos, Sundays, Great Fish and Kei) completed the data set of 14 basins. Their properties are summarized in Table 1.

4.1. Horton's Ratios

[24] For the analysis a 1 km resolution Digital Elevation Model (DEM) was used. Flow of water

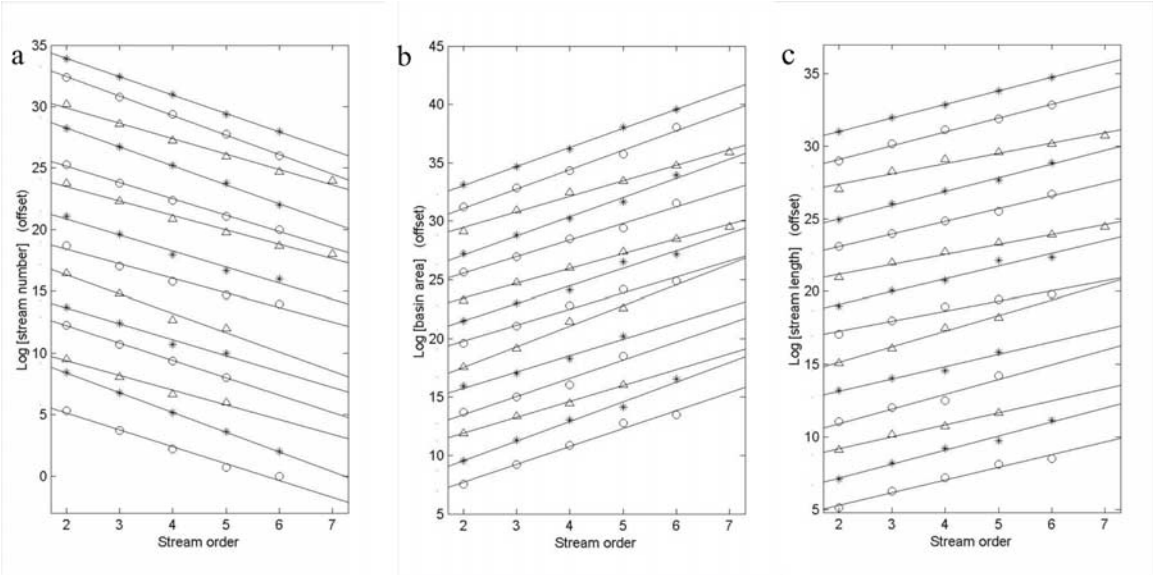

Figure 7. Graphs from which Horton's ratios were obtained: (a) R_n, (b) R_a, and (c) R_l.

over this DEM was modeled, resulting in the construction of the networks. The first task was ordering the streams in each network, as discussed in section 3.1. While first-order basins were identified, the length of the stream draining each such basin, i.e., how far from the watershed the actual stream starts, could not be guessed [see *Montgomery and Dietrich*, 1988]. For this reason, first-order streams were not used in the analysis, which started at second-order streams, which were taken to start at the confluence of first-order basins. Thus when we talk about source streams we actually mean second-order streams. It should be noted that the orders would change if a different resolution DEM was used.

[25] Following the computation of the network, Horton's ratios, and uncertainties in them, were computed for each of the 14 networks using equation (2b), and similar ones for other ratios. Horton's ratios for stream lengths were computed separately for stream segments and mainstream lengths (see section 3.1). At higher orders the two ratios would be similar, but some anomalies will occur for low orders. For 13 of the 14 networks (Hartebees being the exception) mainstream lengths had a better correlation coefficient with order that stream segments did. The average difference in this correlation was 5%. For this reason mainstream length were used throughout this study.

[26] The plots of mean area, length and stream number as functions of order are given in Figures 7a–7c. The y axis values have been offset to enable us to plot all 14 functions on one graph. The individual plots correspond to their position in Table 1, i.e., from Fish river on top to Elands at the bottom. The best fit slopes have also been shown in the graph; these correspond to Horton's ratios, which, along with their uncertainties, are given in Table 2.

[27] Also included in the table are the 2 parameters related to Tokunaga's law, T_1 and R_T. These were computed by plotting $T(\omega_1 - \omega_2)$ as a function of $(\omega_1 - \omega_2 - 1)$, as per equation (4b).

[28] From Figure 7 and Table 2 it is clear that there is no uniform value for any of Horton's ratios. In each network Horton's laws hold, with some small uncertainties (never exceeding 5% of the ratio's value) present. All the mean values, even when the uncertainties are taken into account, fall into typical ranges mentioned in section 3.1. There also exists a strong relationship between R_a and R_n; this is shown in Figure 8. The stars represent values measured for the ratios, with the boxes corresponding to the uncertainties in these values. The solid line is the identity function, on which *Peckham* [1995] showed all points should lie. It is very interesting to note that all the points lie on one side of identity, i.e., $R_a > R_n$. The dash-dot line shows the best linear fit for the 14 points. The intercept is small (0.074), in fact is smaller than the uncertainty associated with it (0.119). This leads us to conclude that $R_n = kR_a$, with k having an observed value of 0.864.

[29] This deviation from the theoretical models of *Peckham* [1995] and *Dodds and Rothman* [1999],

Table 2. Horton's Ratios and Tokunaga's Parameters (With Uncertainties) for the 14 River Networks of This Study

River	R*n*	R*l*	R*a*	R*t*	T1
Fish	4.42 ± 0.00	2.54 ± 0.00	5.10 ± 0.01	2.10 ± 0.03	1.50 ± 0.04
Nossob	4.83 ± 0.01	2.58 ± 0.00	5.26 ± 0.04	2.69 ± 0.07	1.64 ± 0.09
Molopo	3.50 ± 0.02	2.03 ± 0.01	3.76 ± 0.01	1.98 ± 0.03	0.81 ± 0.05
Vaal	4.66 ± 0.01	2.56 ± 0.00	5.11 ± 0.04	2.70 ± 0.09	1.46 ± 0.10
Upper Orange	3.77 ± 0.01	2.40 ± 0.00	4.12 ± 0.04	3.61 ± 0.10	0.62 ± 0.04
Hartebees	3.21 ± 0.01	1.97 ± 0.00	3.53 ± 0.01	1.92 ± 0.01	0.89 ± 0.02
Olifants	3.68 ± 0.04	2.39 ± 0.02	4.42 ± 0.07	1.54 ± 0.16	1.72 ± 0.39
Gourits	3.24 ± 0.03	1.99 ± 0.01	3.91 ± 0.04	1.71 ± 0.10	1.06 ± 0.14
Gamtoos	4.75 ± 0.20	2.92 ± 0.02	5.73 ± 0.11	1.85 ± 0.58	2.71 ± 1.02
Sundays	3.61 ± 0.07	2.33 ± 0.03	4.03 ± 0.07	5.04 ± 1.32	0.49 ± 0.16
Great Fish	4.08 ± 0.00	2.74 ± 0.07	4.68 ± 0.21	3.43 ± 0.34	1.04 ± 0.10
Kei	3.31 ± 0.05	2.28 ± 0.01	3.89 ± 0.01	1.58 ± 0.35	1.01 ± 0.27
Upper Limpopo	4.96 ± 0.00	2.63 ± 0.01	5.35 ± 0.06	2.86 ± 0.11	1.57 ± 0.13
Elands	3.91 ± 0.04	2.37 ± 0.01	4.63 ± 0.06	1.32 ± 0.09	2.30 ± 0.35

which stipulate an identity, is worth commenting on. These models assume network self-similarity, which demands not only the satisfaction of Horton's laws, but also the consistence of Tokunaga's ratios. Section 4.2 shows the latter have a significant error associated with them. Furthermore, very large networks are assumed in the derivations, to allow certain geometric series to converge. It is possible that larger networks (or networks used here with higher resolution DEM) would produce Horton's ratios closer to the identity, though the error coming from Tokunaga's ratios would still exist. It is worth repeating that our observed values fall in the ranges quoted by other studies [e.g., *Abrahams*, 1984], which find R_n between 3 and 5, and R_a between 3 and 6.

[30] The question of what determines the individual values of Horton's ratios is of interest. At first glance it appears the topography does not play a role in determining these. The ratios in the 6 Cape Fold Belt networks vary considerably from each other; for example, the Gourits, which drains similar landscapes right next to the Gamtoos, has ratios which are about two-thirds of those in the latter. Desert "draining" Molopo and Nossob also have very different ratios. Convincing correlations between Horton's ratios and topography parameters do, however, exist. Figure 9 shows a plot of R_n as a function of the mean slope of all second-order streams in the given network. An inverse trend seems to exist. The correlation coefficient of 51.2% puts the probability of regression being real at just under 95%. Two outliers are obvious; these are the Molopo and Hartebees rivers. Interestingly, these are the only networks that have $\Omega = 7$, despite only having fourth and sixth largest drainage areas, respectively. As each of these networks has just two sixth-order streams, we have $n(\omega = 6)/n(\omega = 7) = 2$. This anomalously low value for R_n offsets the regression curve for this ratio; this can be clearly seen in the third and sixth plots in Figure 7a. If these points are not taken into account, the value of R_n for the Molopo would change from 3.50 ± 0.02 to 3.90 ± 0.01, and for the Hartebees network from 3.21 ± 0.01 to 3.56 ± 0.01. These points have been marked as circles in Figure 9. If these, rather than the original points are taken into account, the correlation coefficient goes up to 66.2%, and the inverse dependence of R_n of the mean source stream slope can be stated with 99% confidence.

[31] This inverse correlation between R_n and mean source stream must be treated with caution. It was shown earlier that $R_n \sim R_a$. Furthermore, equation (9)

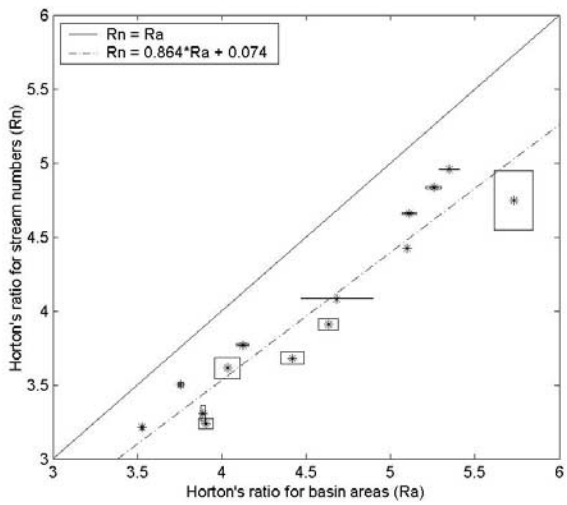

Figure 8. Horton's ratios for stream numbers as a function of Horton's ratio for basin areas. Blocks mark the uncertainty in each value, dashed line is the best fit regression, and solid line is the identity function.

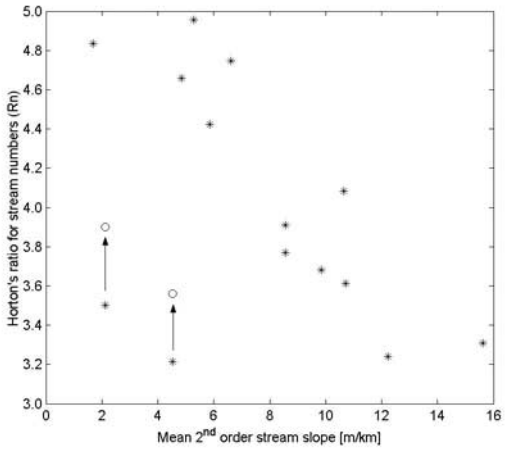

Figure 9. Horton's ratio for stream numbers as a function of mean second-order stream slope. The two circles show how Molopo and Hartebees points would change if the seventh-order point was not taken into account.

inversely correlates basin slope with basin area. Thus if these three regressions hold, it follows that R_a is correlated with a. This is clearly not possible, as Horton's ratios are shown to be scale invariant. The explanation for this apparent contradiction is that the slope-area relation (equation (9)) does not hold at lowest scales. This result, quoted earlier, is also observed in our study: all basins used here were grouped in bins of 20 basins. The mean slope of each bin was plotted against the logarithm of mean basin area, and a very weak inverse correlation of 22.5% was observed. When apparent source streams were removed, the correlation increased to 51.3%. It is possible that the ratio of stream numbers is determined by the slope of basins that are too small to follow the slope area relation. Further research is currently being done on this point.

[32] Other factors were also examined for possible correlation with R_n. Source stream basin relief has a 46.8% correlation coefficient with the ratio. As one would expect slope and relief to be positively correlated, this is not surprising, and as the slope analysis give a better correlation, the slope was concluded to be a first-order factor. Roughness can be quantified using spectral methods [*Turcotte*, 1992]. While the logarithmic plot of the power spectral density against the wave number has a slope corresponding to the topography's fractal dimension, the y intercept (density value at specified wave number, 1 cycle km^{-1} in this case), corresponds to the roughness. These roughness values had a 30% correlation with R_l. This might be considered suggestive, but is definitely not a first-order dependence. Interestingly, the fractal dimensions of the topography showed no traces of correlation with any measured ratio.

[33] Having related R_n to a parameter related to the topography, and having established a relationship between R_n and R_a, it remains to see what determines the value of R_l. To do this, we assume that Horton's laws for stream numbers and stream lengths hold in all networks. We also define a quantity σ_ω, the total length of stream segments of order ω. Furthermore, let σ without a subscript represent the total length of all stream in the network. First-order basins are used in the derivation for completeness, but the reader is reminded that this analysis only used second-order streams and above, so σ_1 in reality represents the sum of second-order streams, σ_2 third order, and so on. Remembering that $l(\omega)$ and $n(\omega)$ represent the mean length and number of stream of given order ω, we have

$$\sigma_1 = l(1) * n(1), \tag{11}$$

$$\sigma_2 = [l(2) - l(1)] * n(2) = [R_l l(1) - l(1)] * \frac{n(1)}{R_n} = \left(\frac{R_l - 1}{R_n}\right) * [l(1) * n(1)], \tag{12a}$$

which can be written

$$\sigma_2 = \left(\frac{R_l - 1}{R_n}\right) * \sigma_1 \tag{12b}$$

and for higher orders, $\omega > 2$

$$\sigma_\omega = [l(\omega) - l(\omega - 1)] * n(\omega) = R_l^{\omega-2}(R_l - 1) * l_1 * \frac{n(1)}{R_n^{\omega-1}}. \tag{13a}$$

This can be expressed in terms of σ_2 or σ_1.

$$\sigma_\omega = \left(\frac{R_l}{R_n}\right)^{\omega-2} * \left(\frac{R_l - 1}{R_n}\right) * \sigma_1 = \left(\frac{R_l}{R_n}\right)^{\omega-2} * \sigma_2. \tag{13b}$$

The total stream length can then be expressed as

$$\sigma = \sum_{i=1}^{\Omega} \sigma_i = \sigma_1 + \sigma_2 * \sum_{i=2}^{\Omega} \left(\frac{R_l}{R_n}\right)^{i-2}. \tag{14}$$

As $R_l < R_n$ the terms in the summation are decreasing. For an infinitely large network this geometric series has a finite sum:

$$\sum_{j=0}^{\infty} \left(\frac{R_l}{R_n}\right)^j = \frac{1}{1 - \frac{R_l}{R_n}} = \frac{R_n}{R_n - R_l} \tag{15}$$

The assumption of an infinite network is obviously unrealistic, but the finite sums in the networks examined here are on average 90% of the right-hand side of equation (15). For now the right-hand side of (15) will be substituted into equation (14). Appendix A shows why this action is justified. Thus, also using equation (12),

$$\sigma = \sigma_1 * \left(1 + \frac{R_l - 1}{R_n} * \frac{R_n}{R_n - R_l}\right) = \sigma_1 * \left(\frac{R_n - 1}{R_n - R_l}\right). \quad (16)$$

An expression for R_l in terms of R_n can then be obtained:

$$R_l = \left(1 - \frac{\sigma_1}{\sigma}\right) * R_n + \frac{\sigma_1}{\sigma}. \quad (17)$$

This expresses Horton's ratio for stream lengths in terms of the ratio for stream numbers. As far as we know, this has not been done before. The other parameter in the equation is the fraction of total stream lengths made up from first-order streams. This fraction is probably not the same for all networks, but is unlikely to vary much. Figure 10 shows the plot of R_l values as function of corresponding R_n. The solid black line corresponds to the best linear regression curve: $R_l = 0.377 * R_n + 0.903$. The dashed line shows the best fit with the condition of the slope and the intercept adding up to unity: $R_l = 0.467 * R_n + 0.533$. This is still an excellent regression; the sum of squares of individual displacements from the line is 0.346, compared to 0.304 for the best fit without the added constraint. Taking the correction from Appendix A into account, this shows that about 56% of all stream lengths are made up of source streams. A simple calculation shows that in the 14 networks 57 ± 3% was made up of the lowest-order streams.

[34] We have thus related the 3 Horton's ratios. The stream number's ratio shows dependence on mean source stream slope. The steeper these basins are, the lower the ratio will be. The ratio for drainage areas is linearly dependant on that for stream numbers. They do not appear to be equal, as *Peckham* [1995] showed should be the case for perfect fractal patterns, instead $R_a = 1.16 * R_n$. This might explains why the observed range for R_a is larger than that for R_n [*Abrahams*, 1984]. This would clearly be impossible if the two always had equal values. Last, a function defining the stream length ratio as a function of stream number ratio was derived. A parameter defined as the fraction of total stream length contributed by source streams appears in that function; further research will be necessary to find out whether that first-order contribution is a constant.

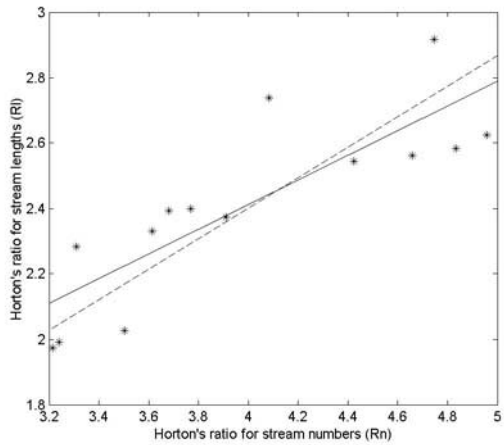

Figure 10. Horton's ratio for stream lengths as a function of Horton's ratio for stream numbers. Solid line shows the best fit regression; the dashed line is the best fit with the constraint of slope and y intercept adding to 1.

4.2. Tokunaga's Ratios

[35] The parameters relating to Tokunaga's law, R_T and T_1, also vary from network to network (Table 1). The uncertainties associated with them are always larger than those associated with Horton's ratios in the particular network. Most of the time these errors are still small, but in some networks, like Gamtoos or Sundays, the error is very large, and it is clear that in these networks Tokunaga's law does not hold.

[36] The fact that Tokunaga's law is not observed in these basins could just be a result of the basins being too small, and there not being enough data to produce statistically viable results. Alternatively, those deviations could represent real phenomena. It was mentioned earlier that these river need to cross the Cape Fold Belt mountains to reach the Ocean. These mountains consist of steep parallel quartzite ridges separated by broad soft shale valleys. The main trunk streams of the network naturally form in the shale valleys, with short streams draining the mountainside feeding them (Figure 11). If the valleys are very long, as many of them are, this will lead to anomalies in stream numbers, causing anomalies in Tokunaga's ratios. These anomalies would thus be inherited from litho-tectonic terrain parameters.

[37] In other networks studied here, the values for R_T and T_1 are well constrained, and are not far

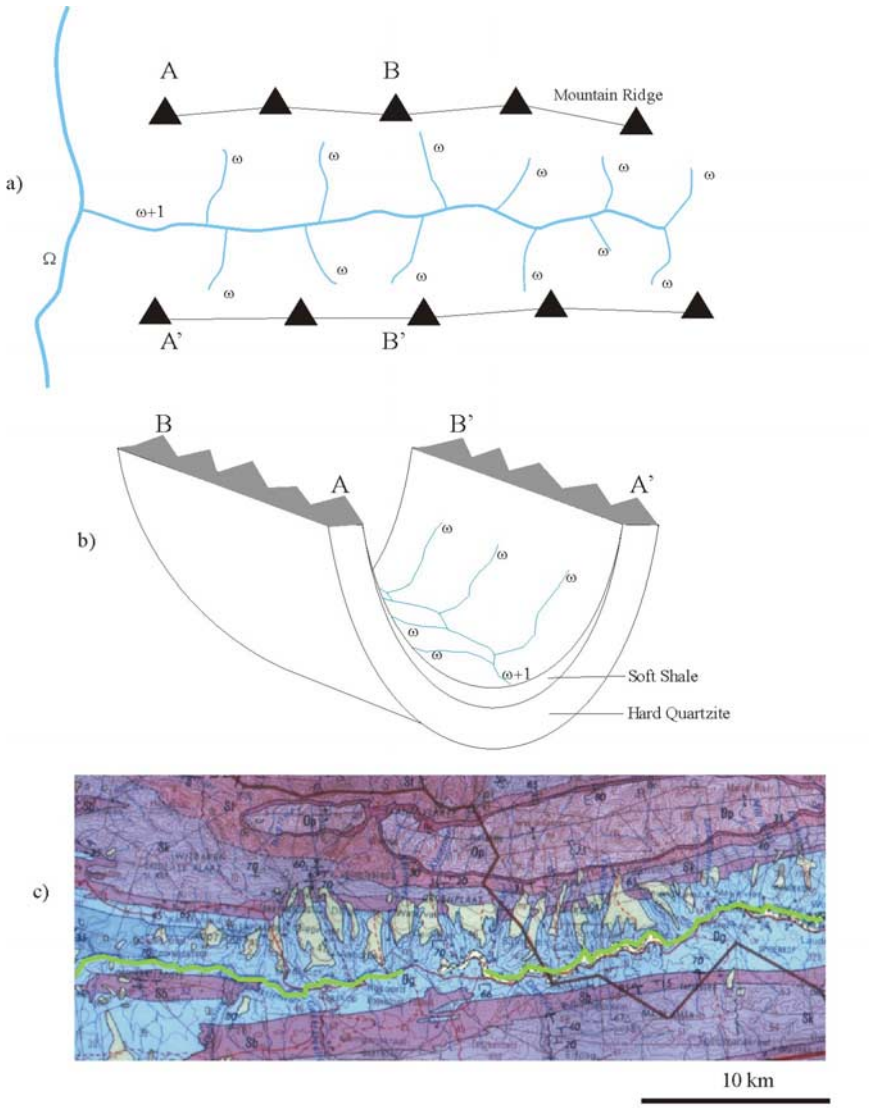

Figure 11. (a) Schematic drainage pattern between two parallel mountain ranges, similar to the pattern found in the Cape Fold Belt. Low-order streams (ω) drain the hard quartzite ridges into the order ω + 1 trunk stream in the shale valley, which in turn drains into the main stream (order Ω) which crosses the mountain belt. Such a drainage pattern will produce larger uncertainties associated with Horton's ratios and would not be expected to obey Tokunaga's law. (b) A schematic cross section through the area illustrated in Figure 11a. (c) Portion of a geological map [*South African Geological Survey*, 1979] of the Swartberg area in the Gourits River drainage basin. The pattern in Figures 11a and 11b is shown; two rivers (marked in green) drain in opposite directions in the shale valley (blue) and are fed by streams draining quartzite and sandstone ridges (different shades of purple) that bind the valley. Yellow represents aeolian sands.

away from their expected expressions in terms of Horton's ratios (right-hand sides of equations (5) and (6)). These are shown in Figures 12 and 13, where the ratios of left-hand side to right-hand side of (5) and (6) are plotted as a function of the network's drainage area. From these graphs it appears that the 2 identities hold for basins above a given size, in this case $\log(a) \approx 11.5$ or $a \approx 100{,}000$ km^2. A study from a more detailed DEM would be necessary to state whether this limit is real, or if the aforementioned lithologic and structural controls cause deviations.

4.3. Hack's Law

[38] The stream length, l, of all basins in the 14 networks as a function of the corresponding basin area, a, is shown on logarithmic axes in Figure 14.

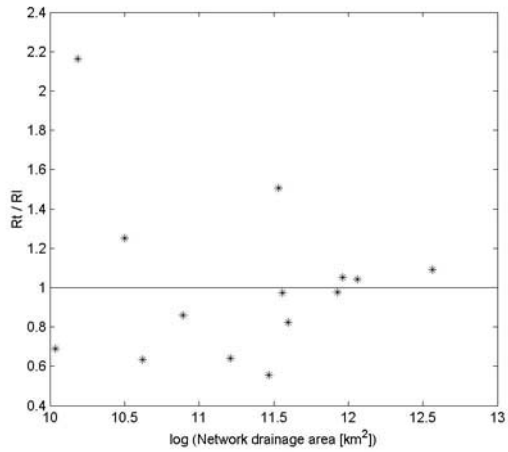

Figure 12. R_T/R_l as a function of network's area. Solid line shows the ratio equal to 1.

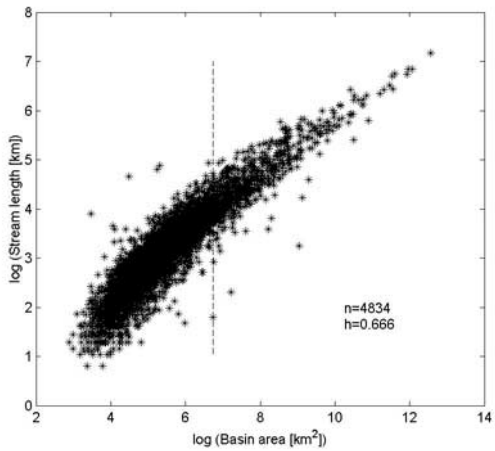

Figure 14. Hack's law plot for combined data (4834 data points). Dashed line shows where the abrupt change in slope occurs.

The best fit slope corresponds to the Hack's exponent for the combined data, and the measured value is $h = 0.666$. This corresponds exactly to $h = 2/3$ measured in the random walk model of *Scheidegger* [1967]. One notices that the graph is slightly convex, which indicates that the value for h is not constant, but decreases with size. The analysis of plots for individual networks (Figure 15) shows that this change is not gradual, but abrupt at a particular threshold. This brings us back to the concept of scaling regimes. *Dodds and Rothman* [2000] suggest networks consist of up to 4 regimes and, for each, Hack's law holds with a different exponent. The regimes they identified were as follows:

[39] 1. Hillslopes: The smallest basins belong to nonconvergent streams running down hillslopes.

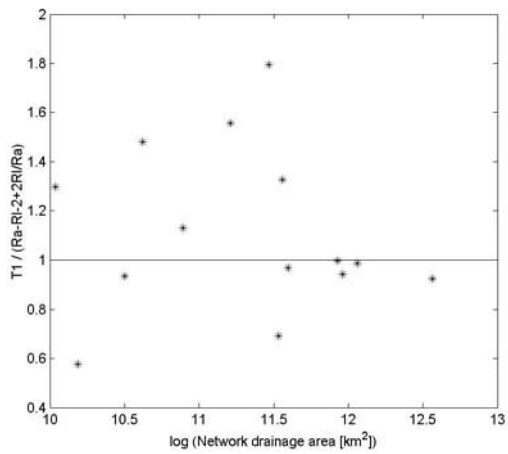

Figure 13. $T_1/(R_a - R_l - 2 + 2R_a/R_l)$ as a function of network's area. Solid line shows the ratio equal to 1.

This regime will be more pronounced in areas that have long, parallel channels. Since streams in this regime do not converge, $l \sim a$, and thus h has a value close to 1.

[40] 2. Short range: This regime starts when streams begin to converge. While the first-order streams are roughly parallel, and second-order ones can be similarly, but to a lesser degree, positioned, at higher orders more sinuous formations can be found. The crossover between the hillslopes and the short range can therefore be quite a gradual one.

[41] 3. Randomness: At larger scales correlations in stream and basin shape decrease, suggesting at this scale streams belong to a random universality class.

[42] 4. Maximal: Eventually, basin reach shapes of geologically constrained maximal basins. As these are controlled by tectonic processes, they are likely to be self similar. Self similarity of basin shapes requires an exponent of 1/2 in the relation between L and a. Combining equations (7) and (8) gives this exponent as h/d. If d has a value of 1.1, as postulated by *Maritan et al.* [1996], $h = 0.55$ would result in a network with self-similar basin shapes. *Dodds and Rothman* [2000] discuss in detail self-similar basins which have d = 1 and h = 0.5. The dependence of basin scaling on this ratio is discussed later in this section, but first we return to the smaller regimes in more detail.

[43] Assuming that the hillslope regime cannot be seen with the 1 km DEM resolution, and that all 14 basins are too small to have properties of maximal

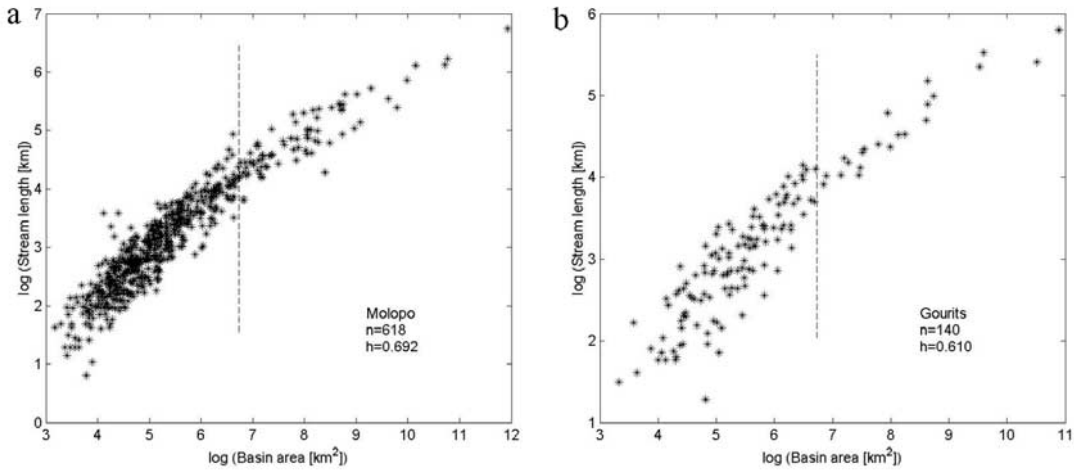

Figure 15. Hack's law plot for (a) Molopo and (b) Gourits networks to show the abrupt change in slope. Dashed line shows where the abrupt change in slope occurs.

continental basins, it follows that the logarithmic plots in Figures 14 and 15 contain only the two regimes in the middle of the scale. It is therefore important to separate the regimes from each other. To do this a statistical analysis was performed. Using the combined data for stream lengths and basin areas from 14 networks (Figure 14), the uncertainty in correlation of the ordered pairs was computed for all basins with the logarithm of the area less than a given value. This maximum was varied between 5 and 10 in steps of 0.01, and the plot of correlation uncertainty as a function of this upper bound is given in Figure 16. The larger the upper bound, the more points are taken into account, and if the plot was a linear regression, increasing the number of points would decrease the correlation uncertainty. This trend is present over $\sim$2 natural orders of magnitude, where the uncertainty starts to increase. The suggestion made here is that at this point a different scaling regime is entered, and we are attempting to correlate points on two adjacent regression lines, resulting in an increase in the uncertainty. The area which corresponds to the lowest correlation uncertainty (log a = 6.73, or $a \approx 800$ km^2) is then the value at which the crossover takes place. The *a-l* ordered pairs from each basin were then separated into the 2 regimes according to which side of the threshold the value for a is. Hack's exponents were then calculated in each basin for the data on either side of the threshold. These are given in Table 3, together with the overall value of h.

[44] As was done with R_n earlier, the values of h from the 14 networks were compared with topography parameters. The best correlation was found to exist between h on either side of the threshold and the roughness of the topography, computed using spectral methods of *Turcotte* [1992]. These are shown in Figure 17. The stars represent the values for h obtained from basins smaller than the threshold, and circles for the ones greater than it. Regression lines have been plotted as well; the results from small basins have 74.9% correlation with the roughness, and the larger ones 54.2%. The regressions can be stated with 99% and 95% confidence, respectively. It is very interesting that with increasing roughness h for small basins decreases, while the h for large basin increases. We

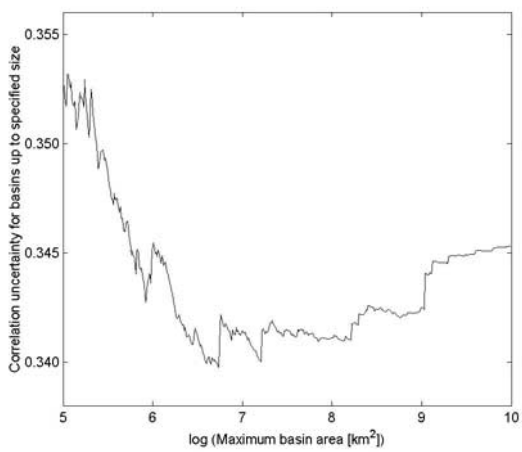

Figure 16. Correlation uncertainty in the Figure 14 plot up to a certain area as a function of that area. The minimum is at log(a) = 6.73; this value is taken as a threshold between short-range and randomness regimes of *Dodds and Rothman* [2000].

Table 3. Hack's Exponent for Each Network, as Well as the Exponent for Subbasins on Either Side of the Regime Crossover Threshold

River	h	h ($\log(a) < 6.73$)	h ($\log(a) > 6.73$)
Fish	0.687	0.776	0.549
Nossob	0.704	0.835	0.477
Molopo	0.692	0.805	0.482
Vaal	0.702	0.782	0.569
Upper Orange	0.644	0.686	0.597
Hartebees	0.671	0.760	0.494
Olifants	0.664	0.692	0.572
Gourits	0.610	0.721	0.474
Gamtoos	0.662	0.709	0.585
Sundays	0.586	0.594	0.597
Great Fish	0.644	0.721	0.590
Kei	0.654	0.744	0.569
Upper Limpopo	0.631	0.717	0.604
Elands	0.680	0.759	0.527

therefore conclude that in the short-range regime the exponent h depends on the roughness of the topography, with rougher surfaces generating lower values of h.

[45] The values observed for h in the two the regimes have implications on basin shapes. Following *Dodds and Rothman* [2001], we define the aspect ratio of a basin

$$\kappa = \frac{L^2}{a}. \tag{18}$$

Using equations (7) and (8), we get

$$\kappa \sim a^{(2h/d)-1}. \tag{19}$$

A similar relation is derived by *Rigon et al.* [1996]. If $(2h/d) > 1$, κ increases with increasing basin area, and therefore large basins appear more elongated. This is the case in the smaller of the 2 regimes studied here; most of the values of h are above 0.7, considerably more than half of the 1.1 expected for d [*Maritan et al.*, 1996]. For $(2h/d) < 1$ elongation is observed as basin size decreases, while $2h = d$ implies self-similarity.

[46] The above-threshold basins from all 14 networks give h close to 0.55, which is exactly half of the 1.1 that *Maritan et al.* [1996] quoted as a value for d. *Dodds and Rothman* [2000] quote a range of 1.0–1.2 for d in real rivers. In their maximal regime these authors quote $h = 0.5$ for self-similarity, but they concede this requires $d = 1$. The mean of the values assembled here for above-threshold h is in fact 0.549, with a standard deviation of 0.049. It therefore appears that basins above the threshold of ~800 km^2 are self-similar. The positive regression of h with the topography roughness cannot be explained without a detailed study of the variations in d. This was not possible from the DEM-generated networks. Real maps will be analyzed for that in due course.

[47] The analysis of the mean value of h for all subbasins in each network was not done here. As there are many basins with $\log(a) < 6.73$, this regime would dominate the average value for the network, and correlations would be much the same as those observed for the short-range regime.

5. Conclusions

[48] The continent of Africa is tectonically and hypsometrically unique, and therefore provides a unique natural laboratory for the study of river network geometry. In this study basic scaling laws of network geometry were analyzed for a set of 14 river basins draining Southern Africa, one of the more unusual geomorphological sections of this continent that is predominantly affected by epeirogenic activity. In each network Horton's laws were observed, but the values for the ratios of stream numbers, stream lengths, and basin areas were different in each network. We found a strong inverse correlation between the value of R_n and mean source stream slope, suggesting this feature of the topography defines the value of the scaling parameter. The other two Horton's ratios were then expressed in terms of R_n. R_a was proportional to the stream number ratio, but about 15% larger than it. This is not what was suggested for self-similar networks, where an identity between the 2 numbers was expected. An expression for R_l was also

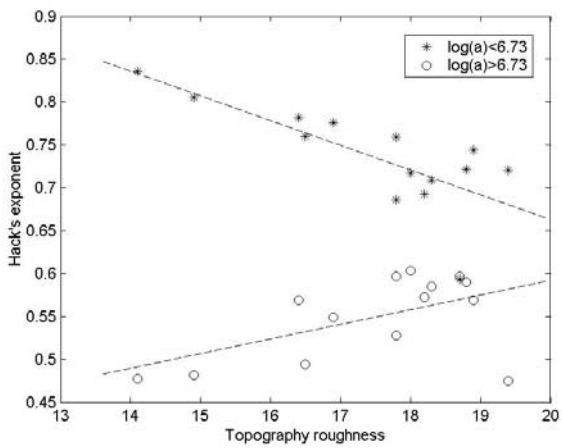

Figure 17. Hack's exponent for basins on either side of the threshold as a function of the roughness of the topography that the network drains.

derived, $[(1 - \sigma_1/\sigma)R_n + \sigma_1/\sigma]$, where σ_1/σ represents the percentage of total stream length contributed by source streams. This relationship was verified for the networks in this study.

[49] Values for side branching ratios (Tokunaga's law) were also obtained, but in some cases the error associated with these was large enough to force a conclusion that this law is not observed. This was only the case for some networks with areas under 100,000 km^2. A more detailed analysis is needed to reveal whether this is a real threshold, or if lithologic and/or structural controls of subbasins result in deviations from this law. Where the error associated with the parameters in Tokunaga's law was small, these parameters corresponded to expressions in terms of Horton's ratios derived for synthetic networks.

[50] Last, Hack's law was observed in the networks of all basins, but a detailed analysis showed that the value for h is not constant in a specific network, but decreases with increasing basin size. This decrease is abrupt rather than gradual. This is consistent with the theory of scaling regimes. Two regimes are visible in the available resolution: short-range and randomness, with the threshold occurring at $a \approx 800$ km^2. The values for h in the short-range regime have an inverse correlation with the roughness of the topography. In all the networks h was large enough to imply basins appear more elongated with increasing area. This would be more pronounced in rivers draining a relatively smooth topography. In the larger of the 2 regimes visible, the values of h are mostly between 0.5 and 0.6. This is the range for which basin shapes are self-similar. There is a positive correlation between this h and topography roughness, but a detailed study of streams' individual fractality, d, is necessary before it can be concluded whether this is a deviation from self-similarity, or a network's adjustment to variation in stream fractality in order to maintain self-similarity.

Appendix A

[51] In section 4.1 it was assumed in derivation of equation (16) that the network is infinite, and therefore the geometric series can be summed as

$$\sum_{j=0}^{\infty}\left(\frac{R_l}{R_n}\right)^j = \frac{1}{1-\frac{R_l}{R_n}} = \frac{R_n}{R_n - R_l}. \tag{A1}$$

However, for a finite network the left-hand side of the above is actually $\sum_{j=0}^{\Omega-2}\left(\frac{R_l}{R_n}\right)^j$.

[52] For the networks used here the finite sum was on average about 90% of the formula for the infinite sum. We therefore write

$$\sum_{j=0}^{\Omega-2}\left(\frac{R_l}{R_n}\right)^j = \frac{0.9 * R_n}{R_n - R_l} \tag{A2}$$

The corrected expression for the sum of all streams then becomes

$$\begin{aligned}\sigma &= \sigma_1 * \left(1 + \frac{R_l - 1}{R_n} * \frac{0.9 * R_n}{R_n - R_l}\right)\\ &= \sigma_1 * \frac{R_n - R_l + 0.9 * R_l - 0.9}{R_n - R_l}\\ &= \sigma_1 * \frac{R_n - 0.1 * R_l - 0.9}{R_n - R_l}.\end{aligned} \tag{A3}$$

Separating Horton's ratios gives

$$R_l * \left(1 - 0.1 * \frac{\sigma_1}{\sigma}\right) = R_n * \frac{1 - \frac{\sigma_1}{\sigma}}{1 - 0.1 * \frac{\sigma_1}{\sigma}} + \frac{0.9 * \frac{\sigma_1}{\sigma}}{1 - 0.1 * \frac{\sigma_1}{\sigma}}, \tag{A4}$$

and an expression for R_l becomes

$$\begin{aligned}R_l &= R_n * \left(\frac{1 - \frac{\sigma_1}{\sigma}}{1 - 0.1 * \frac{\sigma_1}{\sigma}}\right) + \frac{0.9 * \frac{\sigma_1}{\sigma}}{1 - 0.1 * \frac{\sigma_1}{\sigma}}\\ &= R_n * \left(1 - \frac{0.9 * \frac{\sigma_1}{\sigma}}{1 - 0.1 * \frac{\sigma_1}{\sigma}}\right) + \frac{0.9 * \frac{\sigma_1}{\sigma}}{1 - 0.1 * \frac{\sigma_1}{\sigma}}\end{aligned} \tag{A5}$$

Comparing this to equation (17),

$$R_l = \left(1 - \frac{\sigma_1}{\sigma}\right) * R_n + \frac{\sigma_1}{\sigma}, \tag{A6}$$

we see that the slope and the intercept still add up to unity, but the relatively simple $\frac{\sigma_1}{\sigma}$ has been replaced by $\frac{0.9 * \frac{\sigma_1}{\sigma}}{1 - 0.1 * \frac{\sigma_1}{\sigma}}$. Thus the best fit analysis with the constraint of the slope and the intercept adding to 1 was still the correct procedure, but the value of 0.533 corresponded to $\frac{0.9 * \frac{\sigma_1}{\sigma}}{1 - 0.1 * \frac{\sigma_1}{\sigma}}$ rather than $\frac{\sigma_1}{\sigma}$. This, however, is trivial to obtain:

$$\begin{aligned}\frac{0.9 * \frac{\sigma_1}{\sigma}}{1 - 0.1 * \frac{\sigma_1}{\sigma}} &= 0.533\\ \Rightarrow 0.9 * \frac{\sigma_1}{\sigma} &= 0.533 - 0.0533 * \frac{\sigma_1}{\sigma}\\ \Rightarrow \frac{\sigma_1}{\sigma} &= \frac{0.533}{0.9 + 0.0533} = 0.559.\end{aligned}$$

Acknowledgments

[53] We would like to thank Dan Rothman (MIT) for sharing his expertise of river network geometry. Donald Turcotte (U. California) pointed out a number of issues which greatly improved this study. Access to the African river database (used

in Figures 2 and 4) was granted by Mike de Wit of De Beers Group, Centurion. The manuscript benefited greatly from critical reviews by Dan Rothman, Ted Stankiewicz of Hamerkop Scientific Services, and an anonymous reviewer. This research was funded by the National Research Foundation of South Africa.

References

Abrahams, A. D. (1984), Channel networks: A geomorphological perspective, *Water Resour. Res.*, *20*(2), 161–188.

Bootsman, C. S. (1997), On the evolution of the Upper-Molopo drainage, *S. Afr. Geogr. J.*, *79*(2), 83–92.

Brown, C., and R. W. Gilder (1980), Interpretation of African gravity and its implication for the break-up of continents, *J. Geophys. Res.*, *85*, 6443–6455.

Buckle, C. (1978), *Landforms in Africa: An Introduction to Geomorphology*, Longman, New York.

Burke, K. (1996), The African Plate, *S. Afr. J. Geol.*, *99*(4), 341–409.

Coblentz, D. D., and M. Sandiford (1994), Tectonic stresses in the African plate: Constraints on the ambient lithospheric stress state, *Geology*, *22*, 831–834.

Cogley, J. C. (1987), Hypsometry of the continents, *Z. Geomorphol. Suppl.*, *53*, 48 pp.

Cox, K. G. (1989), The role of mantle plumes in the development of continental drainage patterns, *Nature*, *342*, 873–877.

de Wit, M. C. J. (1990), Paleoenviromental interpretation of Tertiary sediments at Bosluispan, Namaqualand, *Palaeontol. Afr.*, *21*, 101–118.

de Wit, M. C. J. (1993), Cainozoic evolution of drainage systems in the north-western cape, Ph.D. thesis, Univ. of Cape Town, Rondebosch, South Africa.

Dodds, P. S., and D. H. Rothman (1999), Unified view of scaling laws for river networks, *Phys. Rev. E*, *59*(5), 4865–4877.

Dodds, P. S., and D. H. Rothman (2000), Scaling, universality, and geomorphology, *Annu. Rev. Earth Planet. Sci.*, *28*, 571–610.

Dodds, P. S., and D. H. Rothman (2001), Geometry of river networks. I. Scaling, fluctuations, and deviations, *Phys. Rev. E.*, *63*, 016115, 1–13.

Doucouré, C. M., and M. J. de Wit (2003), Old inherited origin for the present near-bimodal topography of Africa, *J. Afr. Earth Sci.*, *36*, 371–388.

du Toit, A. L. (1933), Crustal movements as a factor in the evolution of South Africa, *S. Afr. Geophys. J.*, *16*, 3–20.

Fairhead, J. D. (1988), Mesozoic plate tectonic reconstructions of the central South Atlantic Ocean: The role of the West and Central African rift system, *Tectonophysics*, *155*, 181–191.

Frizon de Lamotte, D., B. Saint Bezar, R. Bracene, and E. Mercier (2000), The two main steps of the Atlas building and geodynamics of the western Mediterranean, *Tectonics*, *19*, 740–761.

Hack, J. T. (1957), Studies of longitudinal stream profiles in Virginia and Maryland, *U.S. Geol. Surv. Prof. Pap.*, *294B*, 45–97.

Holmes, A. (1944), *Principles of Physical Geology*, 532 pp., Thomas Nelson, Edinburgh.

Horton, R. E. (1945), Erosional development of streams and their drainage basins: Hydrophysical approach to quantitative morphology, *Bull. Geol. Soc. Am.*, *56*(3), 275–370.

Ijjasz-Vasquez, E., R. L. Bras, and I. Rodriguez-Iturbe (1993), Hack's relation and optimal channel networks: The elongation of river basins as a consequence of energy minimization, *Geophys. Res. Lett.*, *20*(15), 1983–1986.

Lithgow-Bertelloni, C., and P. G. Silver (1998), Dynamic topography, plate driving forces, and the African superswell, *Nature*, *395*, 269–273.

Mandelbrot, B. B. (1967), How long is the coast of Britain? Statistical self-similarity and fractional dimension, *Science*, *156*, 636–638.

Mandelbrot, B. B. (1983), *The Fractal Geometry of Nature*, W. H. Freeman, New York.

Maritan, A., A. Rinaldo, R. Rigon, A. Giacometti, and I. Rodriguez-Iturbe (1996), Scaling laws for river networks, *Phys. Rev. E*, *53*(2), 1510–1515.

Montgomery, D. R., and W. E. Dietrich (1988), Where do channels begin?, *Nature*, *336*, 232–234.

Mueller, J. E. (1973), Re-evaluation of the relationship of master streams and drainage basins: Reply, *Geol. Soc. Am. Bull.*, *84*, 3127–3130.

Partridge, T. C., and R. R. Maud (1987), Geomorphic evolution of southern Africa since the Mesozoic, *S. Afr. J. Geol.*, *90*, 179–208.

Peckham, S. D. (1995), New results for self-similar trees with applications to river networks, *Water Resour. Res.*, *31*(4), 1023–1029.

Pelletier, J. D. (1999), Self-organization and scaling relationships of evolving river networks, *J. Geophys. Res.*, *104*(B4), 7359–7375.

Reeves, C. V. (1972), Rifting in the Kalahari?, *Nature*, *237*, 95–96.

Reeves, C. V. (1978), A failed Gondwana spreading axis in southern Africa, *Nature*, *273*, 222–223.

Rigon, R., I. Rodriguez-Iturbe, A. Maritan, A. Giacometti, D. G. Tarboton, and A. Rinaldo (1996), On Hack's law, *Water Resour. Res.*, *32*(11), 3367–3374.

Rigon, R., I. Rodriguez-Iturbe, and A. Rinaldo (1998), Feasible optimality implies Hack's law, *Water Resour. Res.*, *34*(11), 3181–3190.

Rodriguez-Iturbe, I., and A. Rinaldo (1997), *Fractal River Basins: Chance and Self-Organization*, Cambridge Univ. Press, New York.

Sahagian, D. (1988), Epeirogenic motions of Africa as inferred from Cretaceous shoreline deposits, *Tectonics*, *7*(1), 125–138.

Scheidegger, A. E. (1967), A stochastic model for drainage patterns into an intramontane trench, *Int. Assoc. Sci. Hydrol. Bull.*, *12*(1), 15–20.

Schorghofer, N., and D. H. Rothman (2001), Basins of attraction on random topography, *Phys. Rev. E*, *63*(2), 026112, 1–7.

Schorghofer, N., and D. H. Rothman (2002), Acausal relations between topographic slope and drainage area, *Geophys. Res. Lett.*, *29*(13), 1633, doi:10.1029/2002GL015144.

South African Geological Survey (1979), Map 3322 (Oudtshoorn), 1:250,000 Geological Series, Pretoria, South Africa.

Strahler, A. N. (1957), Quantitative analysis of watershed geomorphology, *Eos Trans. AGU*, *38*(6), 913–920.

Tarboton, D. G., R. L. Bras, and I. Rodriguez-Iturbe (1989), Scaling and elevation in river networks, *Water Resour. Res.*, *25*(9), 2037–2051.

Tinker, J. H., and M. J. de Wit (2004), Balancing erosion and deposition on and around southern Africa since Gondwana break-up, in *Geoscience Africa 2004 Abstract Volume*, pp. 634–635, Univ. of Witwatersrand, Witwatersrand, South Africa.

Tokunaga, E. (1966), The composition of drainage network in Toyohira River Basin and the valuation of Horton's first law, *Geophys. Bull. Hokkaido Univ.*, *15*, 1–9.

Tokunaga, E. (1978), Consideration on the composition of drainage networks and their evolution, *Geogr. Rep. Tokyo Metrop. Univ.*, *13*, 1–27.

Tokunaga, E. (1984), Ordering of divide segments and law of divide segment numbers, *Trans. Jpn. Geomorphol. Union*, *5*(2), 71–77.

Turcotte, D. L. (1992), *Fractals and Chaos in Geology and Geophysics*, Cambridge Univ. Press, New York.

Wellington, J. H. (1955), *Southern Africa—A Geographic Study*, vol. I, *Physical Geography*, Cambridge Univ. Press, New York.

White, R., and D. McKenzie (1989), Magmatism at rift zones: The generation of volcanic continental margins and flood basalts, *J. Geophys. Res.*, *94*, 7685–7729.

Zoback, M. L., et al. (1989), Global patterns of tectonic stress, *Nature*, *341*, 291–298.